Journal of Geological Remote Sensing

Journal homepage: https:// jgrs.kgut.ac.ir

Evaluation of subpixel spectral methods for identification and change detection of secondary iron minerals

Aliyeh Seifi[1] , Mahdieh Hosseinjanizadeh[1,*],·Hojjatolah Ranjbar[2], Mehdi Honarmand[1]

[1] *Department of Ecology, Institute of Science and High Technology and Environmental Sciences, Graduate University of Advanced Technology, Kerman, Iran*
[2] *Department of Mining Engineering, Shahid Bahonar University, Kerman, Iran*

Article Info	Abstract
Keywords: Subpixel methods Change detection Iron mineral Darrehzar mine	The main objective of this research is to discriminate secondary iron minerals and investigate changes caused by their relocation during mining activities using multispectral satellite data collected over an 11-year period. To achieve this aim, MF and CEM performed using USGS library spectra, field spectra and image spectra to identify secondary iron minerals and then the best result of the mineral identification stage implemented for changes detection of secondary iron minerals. The results of secondary iron minerals identification by MF method and images spectra have compatibility with the field data and laboratory analysis, so that the goethite is the most abundant secondary iron mineral in Darrehzar mine area. The change detection algorithm at the study area showed that mining activities and geochemical conditions cause change in the surface by transferring secondary iron minerals. The employed method including identifying minerals and detecting change of them allows users to find an effective technique for identifying the target material and apply it in the subtraction algorithm for change detection. Applying this method can be suggestions for future research in target change detection.

1. Introduction

Mining activities cause changes in the Earth's surface by transferring rocks and surficial minerals such as ferruginous minerals in gossans (mostly hematite, goethite, and jarosite) and as a result of it, tailing damp and mine waste are produced (Atapour and Aftabi, 2007; Petropoulos et al., 2012; Vali et al., 2014) that could be detected and monitored using remote sensing instruments and techniques. Remote sensing instruments and images are usable for identifying reserves of ores, monitoring environment of mines, surveying tailings and identifying acid mine drainage (Paterson, 1997). Landsat series of satellites which have served remote sensing communities since the early 1970s, are helpful in monitoring the Earth's surface. Landsat 8 was launched in 2013, provides data for the VNIR, and shortwave infrared (SWIR) spectral bands with a 30 m spatial resolution as well as a 15 meter for panchromatic band in Operational Land Imager (OLI) sensor (Department of the Interior U.S. Geological Survey, 2016). Advanced Land Imager (ALI) sensor that was built to provide essential data for Landsat 8 mission, was successfully launched from Vandenberg Air Force Station, California on Earth observation (EO-1) satellite on November 21, 2000 (Beck, 2003; Lencioni et al., 2005). This sensor, which is very similar with Landsat especially in the visible portion, contains nine multispectral bands with 30 m spatial resolution (in VNIR and SWIR portions) (Mendenhall et al., 1998).

Various spectral techniques, such as Matched Filtering (MF), Constrained Energy Minimization (CEM) have been used to detect clay minerals bearing zones and Fe-minerals bearing area in order to map mineralized altered areas by advanced spaceborne thermal emission and reflection radiometer (ASTER) and Landsat multispectral images (Rowan et al, 2003; Zhang et al, 2007; Gabr et al, 2010; Ghulam et al, 2010; Sadeghi, et al, 2013; Alimohammadi et al, 2015; Beiranvand Pour et al, 2015; Mokhtari and Seifi, 2021; Seifi et al., 2021). Many researchers have been involved implementing statistical (principal component analysis (PCA)) and spectral (mixture tuned matched filtering (MTMF) and linear spectral unmixing (LSU)) on ASTER, Landsat and Hyperion data for mapping ferruginous caps (gossans) and alterations zones in Sarcheshmeh and Darrehzar mines (Ranjbar et al, 2004; Beiranvand Pour et al, 2013; Hosseinjani Zadeh et al, 2014a; Hosseinjani Zadeh et al, 2014b; Abedi et al, 2015).

Many researchers have been involved in determining changes in mining areas in the Jharia coalfield (India), the central Appalachians, the Rutenburg mining region, Amazon, Ghana, the Greek island of Milos, Turkey and Germany using time series of Landsat, IRS, Quickbird and Worldview images (Prakash and Gupta, 1998; Ololade et al., 2008; Townsend et al., 2009; Schroeter and Gläβer, 2011; Petropoulos et al., 2012; Lobo et al., 2014; Yucel et al., 2014; Basommi et al., 2015). However these multispectral images are mainly used for mapping land use and land cover in mining areas (Prakash and Gupta, 1998; Ololade et al., 2008; Basommi et al., 2015), less attention is paid for detection of changes in minerals exposure for monitoring tailings. On the other hand, even though different algorithms were used for change detection, rare publications are available for mapping minerals through known spectral based algorithm such as spectral angle mapper (SAM) and matched filtering (MF) (Kruse et al., 1993; Harsanyi and Chang, 1994; Boardman et al., 1995; Wen and Yang, 2009; Valizadeh Kamran and Khorrami, 2018). However, many researchers reported the importance of MF and CEM in mineral identification (Rowan et al., 2003; Zhang et al., 2007; Gabr et al., 2010; Sadeghi et al., 2013; Alimohammadi et al., 2015; Seifi et al., 2016; Mokhtari and Seifi, 2021; Seifi et al., 2021), its importance for discrimination of change detection is paid less attention.

Although many remote sensing studies conducted in the Darrehzar porphyry copper mine, in Kerman copper belt (KCB), south east of Iran (Ranjbar et al., 2004; Beiranvand Pour et al., 2013; Shahriari et al., 2013; Hosseinjani Zadeh et al., 2014a; Hosseinjani Zadeh et al., 2014b; Abedi et al., 2015; Seifi et al., 2016; Seifi et al., 2017; Seifi et al., 2019a; Seifi et al., 2019b), there are no investigations focuses on changes created by ore materials relocation using satellite images in this area. Hence the main objective of this research is to investigate changes created due to mining activities and discriminate iron minerals variation such as hematite, jarosite and goethite through the employed MF and CEM subpixel spectral techniques using multispectral satellite data at the Darrehzar mine during a 11-year period. For this purpose, MF and CEM are performing using United States Geological Survey (USGS) library spectra, field spectra and image spectra and then change detection of secondary iron minerals is going to implement according to the best result of the following stage.

2.Study Area

The Darrehzar porphyry copper deposit is located 80 km northeast of Sirjan in Kerman province and eight km south of well-known Sarcheshmeh porphyry copper deposit. This area is situated in the Urumieh–Dokhtar magmatic belt of Iran (Sahand- Bazman) and is a part of the Kerman copper belt, namely Dehaj-Sarduiyeh magmatic arc (Figure 1).

In the years 1969 and 1970, a former Yugoslavian geological team conducted an initial exploration investigation in the Darrehzar region on behalf of the Iranian Geological Survey. They carried out geological, geophysical, and geochemical investigations before drilling 24 wells and two tunnels for exploration. On the basis of these facts, they calculated the Cu/Mo reserve. Additional drilling and new exploration activities started in 1993, and overburden removal efforts began in 1995. In order to produce the necessary ore for semi-industrial bioheap leaching studies, extraction operations have been carried out since May 2004 for a period of one year. Due to the presence of sulfide-bearing minerals, water infiltration, and oxidant bacteria at the deposit site, acid mine drainage was produced (Moazzen zadeh et al., 2006). Official exploration efforts for ore reserve estimation and mine design began in 2006, and an operational license was then secured from the Kerman province's Industries and Mines Organization in 2007 (Yazdanpanah, 2011; Hosseinjani Zadeh, 2013; Parsapoor, 2014).
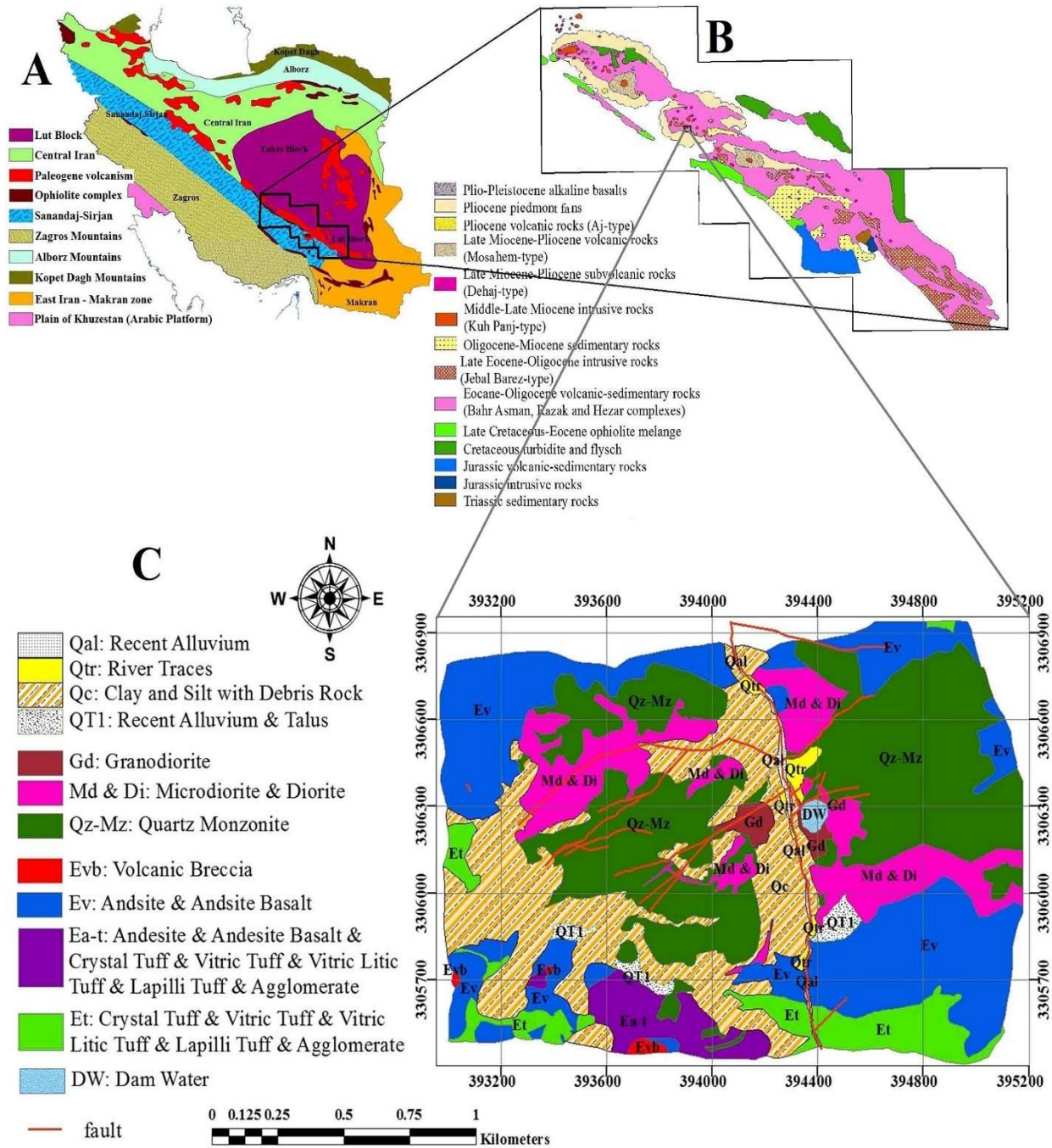
Figure 1. A) A structural-sedimentary map of Iran (modified after Moeen Vaziri, 2004), B) geological map of Dehaj-Sarduyeh (modified after Nateghi and Hezarkhani, 2013), and C) geological map of the Darrehzar porphyry copper deposit (modified after Alizadeh Sevari and Hezarkhani, 2014).

The Darrehzar porphyry is situated in a diorite diorite–quartz pluton of Oligocene–Miocene age which intrudes an Eocene Volcanic–Sedimentary complex consisted mainly of volcaniclastics, andesite, trachyandesite and sedimentary rocks. Hydrothermally altered rocks are highly fractured, and supergene alteration has produced extensive limonite and leaching of sulfide, giving a characteristic reddish or yellowish color to the altered rocks (Geological Survey of Iran, 1973). Propylitic and phyllic alterations are dominant in surface rocks with sporadic small areas of argillic alteration. Propylitic alteration is well developed in the area and extends a few hundred meters around the central phyllic zone. The phyllic alteration persists below the oxidation zone and is characterized by enrichments in Si, Al and K, and depletions in Na, Ca, Mg and Mn (Ranjbar et al., 2001). Potassic alteration is not observed on surface, possibly as a result of a surface related weathering or intense phyllic overprint (Geological Survey of Iran, 1973).

3.Materials and Methods

## 3.1.Satellite data

In order to investigate the mineral identification and change detection in Darrehzar area, images were selected in a manner to cover two periods in summer (normally AMD observed in summer) (Guo et al., 2013; Navarro Torres et al., 2011); a)

2004 (before official exploration activities (2005) and after reported acid mine drainage pollution (2003) (Hosseinjani Zadeh, 2013; Moazzen zadeh et al., 2006)) and b) 2015 (before the first implemented field investigation by authors at the study area). The image of 2015 was related to OLI sensor of Landsat 8 which has been acquired on the 9 August 2015 and was downloaded from the USGS website. Unfortunately, there was no suitable Landsat (ETM + and TM) images in 2004 for the study area. Therefore, the ALI image, which is similar to Landsat in terms of sensor design, platforms orbital characteristics, spatial and spectral resolution, was chosen (Department of the Interior U.S. Geological Survey, 2016). The ALI image, which is contemporary in season with the OLI, was acquired on the 26 July 2004 from USGS website.

3.2. Field data

Field reconnaissance was conducted for collecting rock samples at the study area in 2016. Fresh/weathered and representative oxidized rocks samples were collected from different parts of mining pit and tailing damps through a random punctual sampling and their positioning were recorded by global position system (GPS) Oregon 650. These samples were collected from different areas of the mining pit and waste dumps of the Darrehzar mine (Figure 2).
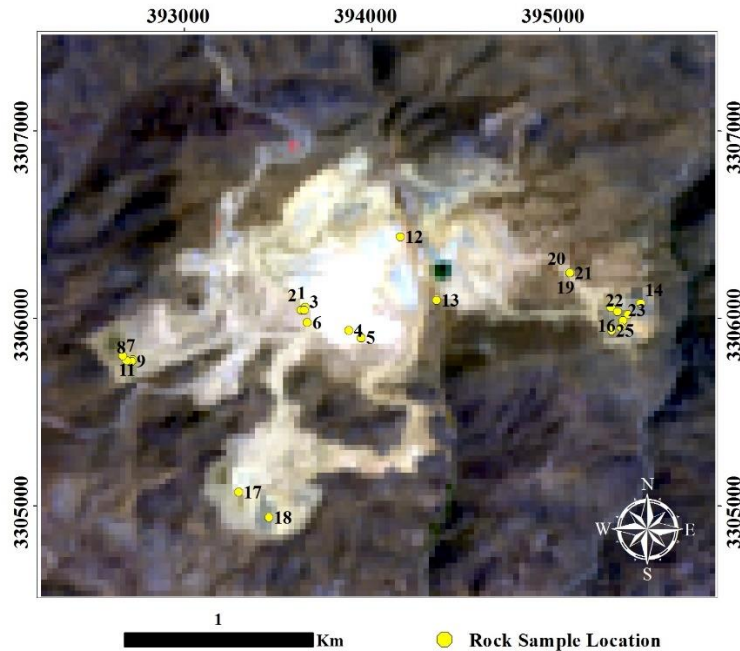
Figure 2. Location of rock samples which were plotted on the color composite of OLI image (each number on the figure indicate sample number such as; 1: Da1, 2: Da2, 3: Da3, 4: Da4, 5: Da5, 6: Da6, 7: Da7, 8: Da8, 9: Da9, 10: Da10, 11: Da12, 12: Da21, 13: Da24, 14: Da26, 15: Da27, 16: Da28, 17: SD, 18: SD1, 19: NED, 20: NED1, 21: NED2, 22: ED1, 23:ED2, 24: ED3, 25:ED4).

Collected samples were sealed in clean polythene bags and kept for further analysis (spectroscopy studies and X-ray diffraction). Spectroscopy of rock samples were carried out in a laboratory by an analytical spectral device (ASD) FieldSpec®3 spectroradiometer as well as spectral processing and mineral recognition were conducted using PIMA View V.3.1., Specmin-PRO V.3.1, and ENVI 5.3® software. The average percentage of minerals in results of PIMA View and Specmin-PRO for the spectra of each sample was considered as the final percentages for minerals in samples. The XRD spectra of powdered samples with the best spectral features were obtained with a Philips PW 1800 diffractometer using Cu–Kα radiation (Kα = 1.542 Å), operating at 40 kV and beam current of 30 mA. Moreover, previous researches (Abdolzadeh, 2005; Atapour and Aftabi, 2007; Keshavarzi, 2006) in the study area were used to

validate results of image processing of ALI data (2004).

3.3.Pre-processing:

Applying atmospheric correction algorithms is a crucial step in the pre-processing process because atmospheric water vapor and particles cause noise in the digital values of the pixels in remotely sensed images (Hosseinjani Zadeh, 2013). Therefore, the ALI and OLI data were corrected using the Fast Line-of-sight Atmospheric Analysis of Spectral Hypercubes (FLAASH) method. The implemented atmospheric correction removes atmospheric effects on image pixels and retrieves spectral reflectance of Earth`s surface from multispectral radiance images (ITT Visual Information Solutions, 2008). So level 1T of ALI and OLI images were downloaded from the USGS website, they registered and were geometrically accurate by

1:25000 topographic map and stream layer of study area.

3.4. Endmember extraction:

In order to identify secondary iron minerals including; hematite, goethite and jarosite, and detect changes for them in aforementioned period, the MF and CEM algorithms were implemented on

ALI and OLI images separately using spectra of these minerals from USGS spectral library. Whereas there are many spectra for each mineral in the USGS spectral library hematite2, goethite3, and jarosite1 spectra were chosen according to the research of Hosseinjanizadeh et al. (2014b) (Figure 3A).
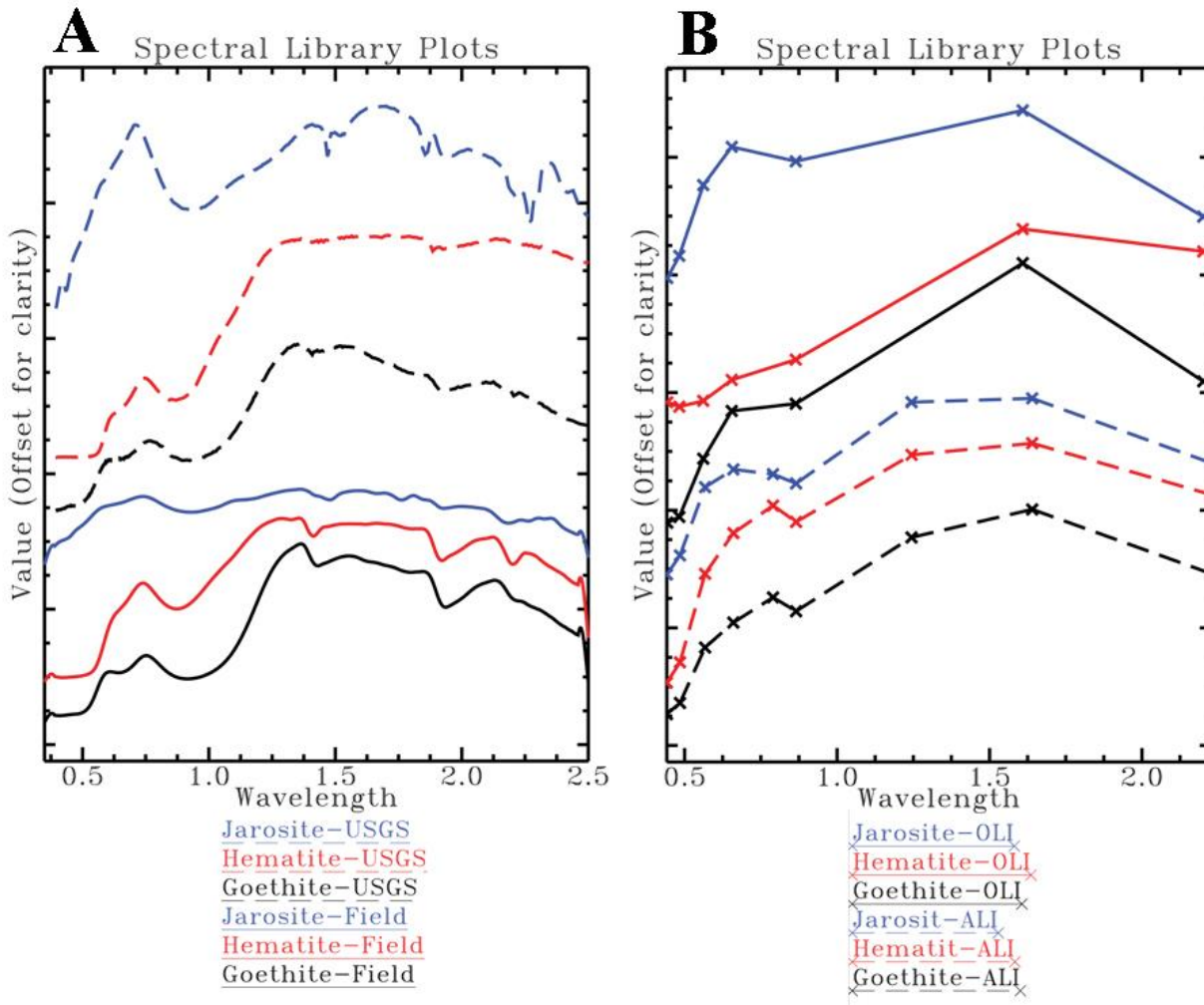
Figure 3. The USGS, field and image spectra of secondary iron minerals such as jarosite, hematite and goethite: A) The USGS and field spectra; B) The OLI and ALI image spectra.

As mentioned above, minerals in rocks samples were identified by spectroscopy measurement using an ASD FieldSpec®3 spectroradiometer in a laboratory. So that samples are mixtures of different

minerals and less abundant minerals may not be observed in one single measurement, multiple spectra were acquired at the laboratory from rocks samples taking into account (95 spectra from 26

samples). The spectral processing and mineral recognition were carried out by PIMA View V.3.1., Specmin-PRO V.3.1, and ENVI 5.3® software.

Goethite, hematite and jarosite in rock samples are identified using absorption features in ASD spectra because of crystal field transitions of ferric/ferrous iron in Fe-minerals, OH stretch in secondary iron minerals and Fe-OH stretch in jarosite (Zabcic 2008; Hosseinjanizadeh et al. 2014b; Seif et al. 2017). At the present study, absorption features of crystal field transitions in ferric/ferrous iron (0.62-0.63 and 0.90-0.93 μm in goethite, and 0.87 μm in hematite) and OH stretch (1.41 and 1.92 μm in hematite, and 1.42 and 1.93 μm in goethite) combinations were used for identifying of goethite and hematite in rock samples. Absorption features associated with crystal field transitions of ferric/ferrous iron (0.44 μm in jarosite) and Fe-OH (2.26 μm in jarosite) were considered as jarosite (Figure 3A). Moreover, Al-OH absorption feature (2.20 μm) observed in ASD spectra could be because of the presence of clay minerals in measured samples (Hosseinjanizadeh et al., 2014b, Seifi et al., 2019a).

For pure spectra extraction of images' pixels, at first, inherent dimensionality of image data was determined using Minimum Noise Fraction (MNF) rotation to separate noise in the data, and to decrease the computational requirements for next processing. Then Pixel Purity Index (PPI) were performed to segregate the purest pixels in the Landsat 8 and ALI multispectral images (Research Systems Inc., 2004). Corresponding spectra of bright pixels in the PPI image and their similarity with resampled spectra of spectral library were used for extracting the purest spectra..Moreover, Sequential Maximum Angle Convex Cone (SMACC) spectral tool was carried out to find spectral image endmembers and to help the pure spectra extraction process (Research Systems Inc., 2004).

There are absorption features associated with crystal field transitions of ferric/ferrous iron (0.43-0.48, 0.50-0.67 and 0.85-0.94 μm) in band 2 ALI and OLI for jarosite, in band 3 OLI for hematite, and in band 5 OLI and band 6 ALI for jarosit, goethite and hematite. As well as, ALI and OLI spectra presented absorption characteristics of OH stretch (1.9 μm) in band 9 ALI and band 7 OLI for three mentioned minerals (Figure 3B).

3.5.Mineral Identification:

Goethite was chosen for selecting the best method because it is the most stable Fe-mineral in acid mine drainage participates and gossans in mining area (Atapour and Aftabi, 2007; Singh et al., 1999). In the present research, CEM and MF subpixel spectral techniques were implemented using goethite spectrum of USGS spectral library, OLI image goethite spectrum, and field goethite spectrum on Landsat 8 (OLI) data. MF technique is a procedure implements a partial spectra unmixing to evaluate the user-defined endmembers abundance from a set of reference spectra for mapping the surface minerals. In fact, this method minimizes the response of the composite unknown background by projecting vector of each pixel onto a subspace that is orthogonal to the background spectra and then maximizes the response of the known end-member by comparing the residual pixels to each of the reference spectra and finally matches the known signature (Harsanyi et al, 1994; Boardman et al, 1995; Rowan et al, 2003). CEM technique is a performance of matched filtering methods in the hyperspectral analysis context. CEM applies a finite impulse response filter (a linear operator) to pass through the desired target while minimizing output energy of background. A correlation or covariance matrix is used for characterization of the component unknown background and increased the contrast between the target and background spectra (Farrand and Harsanyi, 1994; Farrand and Harsanyi, 1997;

Resmini et al, 1997; Settle, 2002; ENVI 5.3 online help). Digital Numbers (DNs) of CEM and MF image pixels present relative percentage of interest materials per pixel, as a result they were classified in three groups, 5% - 20% (low value), 20% - 50% (medium value), and 50% - 100% (high value) according to ASD and XRD data in the research of Seifi et al. (2019a). The best results of CEM and MF subpixel spectral techniques corresponding the ASD data was chosen as the best method for next stage, mineral identification. The best method was used to identify secondary iron minerals containing, hematite, goethite, and jarosite by ALI and OLI data. The results of secondary iron minerals identification were classified also in three groups, 5% - 20% (low value), 20% - 50% (medium value), and 50% - 100% (high value). The results of OLI image validated by ASD FieldSpec®3 spectroradiometer data (Table 1). The results of ALI image validated by information in previous researches (Abdolzadeh, 2005; Atapour and Aftabi, 2007; Keshavarzi, 2006) in study area.

3.6. Change Detection

The employed method for change detection of secondary iron minerals which is practical to identify change of the target material includes three phases, method selection, target identification and change detection. The method allows users to find an effective technique for detecting the target material and apply it in the subtraction algorithm for change detection. The gray-scale MF images of following stage were used for detecting hematite, goethite and jarosite changes in an 11-year period between 2004 (ALI data) and 2015 (OLI data). For this purpose, differences between MF images of secondary Fe-minerals are computed by subtracting the MF image of 2004 from MF image of 2015 and classes are determined by applying the certain value of statistical threshold. In order to select threshold in subtraction algorithm, a no change class should be surrounded by an equal number of

positive and negative classes between -1 and +1 (Research System Inc., 2004). So that, the same values of statistical data (0.2 and 0.5) for classifying secondary iron minerals images in following stage were used as statistical threshold.

4. Results and Discussion

4.1. Method Selection

Iron minerals changes created by mining activities investigated through the employed MF and CEM subpixel spectral techniques using multispectral satellite data at the Darrehzar mine during a 11-year period. Goethite was used to select the best method for next stage, mineral identification, because it is one of the most stable secondary iron minerals in a wide range of pH (Seifi et al., 2019a; Singh et al., 1999). Goethite was detected using MF and CEM methods with the help of USGS library, image and Field spectra to choose the best method for identifying secondary iron minerals. The results of goethite identification were classified into three categories, 5%-20% (low value), 20%-50% (medium value), and 50%-100% (high value). Goethite is only found in the mining area, according to the results of the MF method's detection by the USGS spectral library and Field spectra, therefore only 5 to 20% of the desired pixels contain goethite. (Figure 4A and C). Additionally, the results of goethite identification using the CEM method by the USGS spectrum library and Field spectra show that this mineral is found in the mining area with a medium value (20 to 50%) and in the vicinity of the mine with a low value (5 to 20%). (Figure 4D and F). In the results of detecting goethite using MF and CEM methods by image spectra, this mineral is identified in the mining area and also around the mine with low (5 to 20%), medium (20 to 50%) and high values (50 to 100%). (Figure 4B and E). In the results of the MF method by the OLI image spectrum are presented that there is goethite in the mining area

with low, medium and high values, so that the highest value of goethite is located in the mine pit, and the tailings dumps show medium and low values (Figure 4B). The results of the CEM method by the OLI image spectrum reveal the low, medium and high values of goethite, so that there is the high value of goethite in the mining pit, and the medium and low values of goethite are situated in a wide

area around the mine (Figure 4E). Among the results of the six methods, the result of the MF method by image spectra has compatibility with the field data and laboratory analysis, so that the goethite mineral is observed in most of the collected samples (Figure 2 and Table 1).
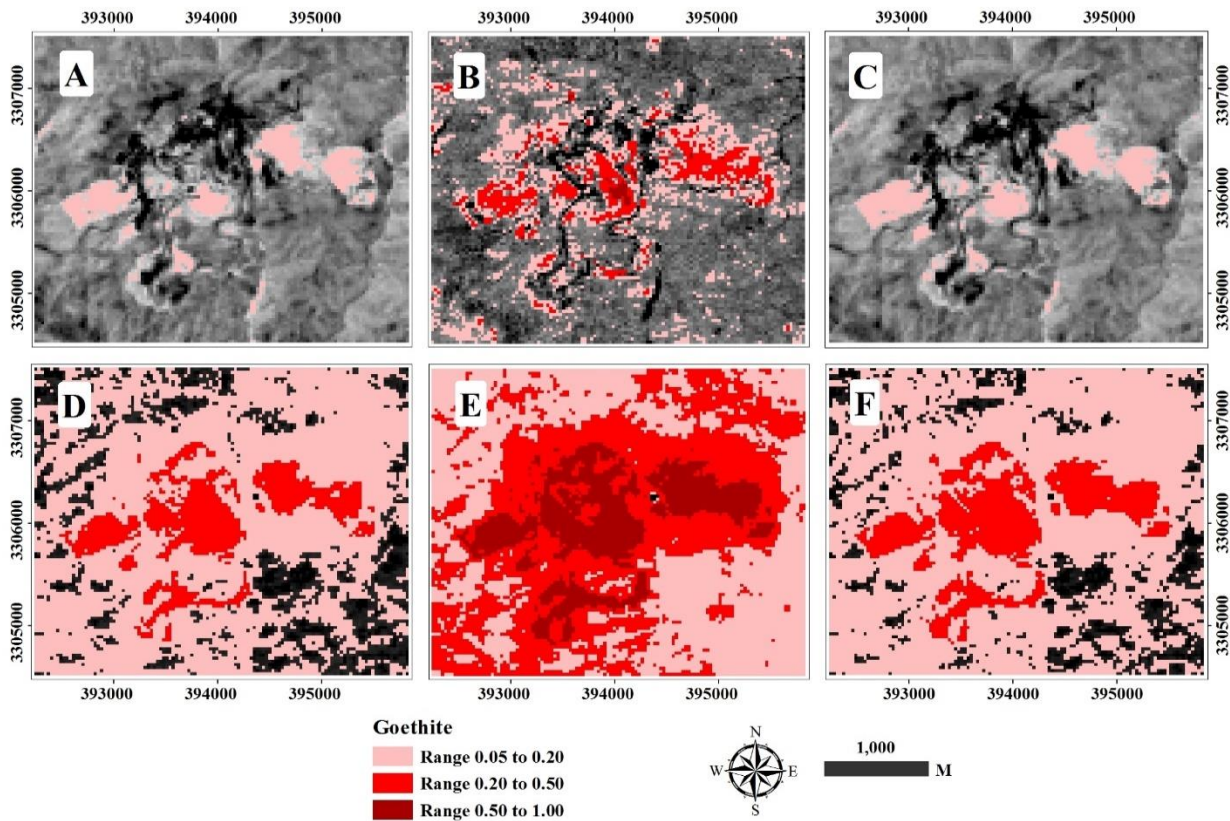
Figure 4. Spatial distribution maps of Goethite in the study area created by A) the MF method and USGS spectrum; B) the MF method and OLI image spectrum; C) the MF method and field spectrum; D) the CEM method and USGS spectrum; E) the CEM method and OLI image spectrum; F) the CEM method and field spectrum.

4.2. Mineral Identification

Secondary iron minerals containing goethite, hematite and jarosite were identified by MF method using images spectra. The spectra of

aforementioned minerals were extracted from ALI and OLI satellite images (Figure 3B) and used for detecting secondary iron minerals. Goethite is the most abundant secondary iron mineral in Darehazar

mine area, and it presents a few changes between 2004 to 2015 (Figure 5A and D). Hematite is mainly detected with moderate (20-50%) and high (50-100%) values along the Darrehzar River, which intersects the Darrehzar mine into two parts, in 2004 image (ALI) (Figure 5B). But it is identified by low value (5 to 20%) in the mine area and also by medium value (20 to 50%) in some central parts of the mine in the OLI image (2015) (Figure 5E). Jarosite is detected using the ALI satellite image

(2004) in the mining area with low (5 to 20%), medium (20 to 50%) and high (50 to 100%) values, so that the low amounts of jarosite is detected in a wider area than the medium and high values in Darrehzar mine (Figure 5C). Moreover, this mineral is identified with medium and high values in a more widespread area than the low value of jarosite in the Darrehzar mine in the 2015 image (OLI), and mostly these values correspond to the pit of Darrehzar mine (Figure 5F).
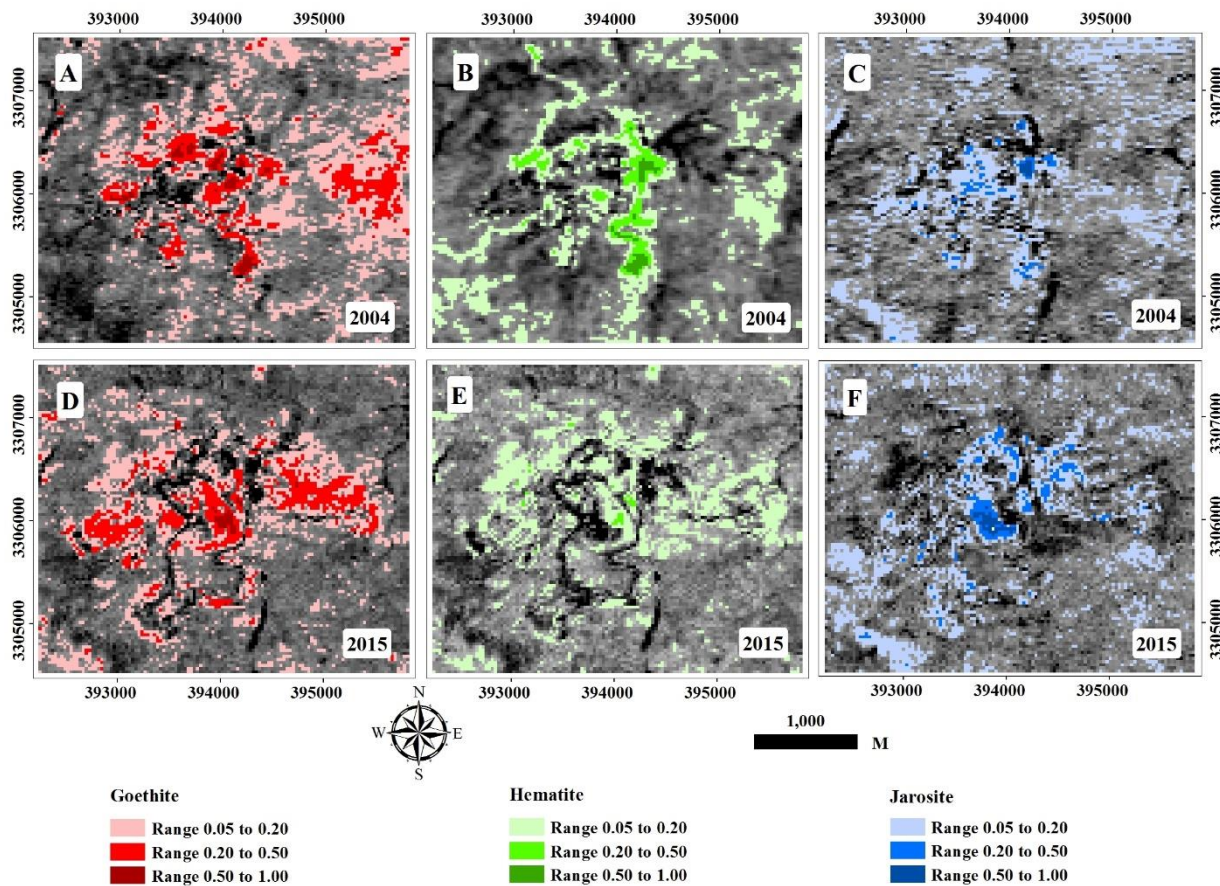
Figure 5. A) Result of the MF method and ALI image spectrum for goethite identification; B) Result of the MF method and ALI image spectrum for hematite identification; C) Result of the MF method and ALI image spectrum for jarosite identification; D) Result of the MF method and OLI image spectrum for goethite identification; E) Result of the MF method and OLI image spectrum for hematite identification; F) Result of the MF method and OLI image spectrum for jarosite identification.

Field observations and laboratory analysis of collected samples from the mine confirm the image processing results.

Previous studies approve the results of ALI images processing so that Abdolzadeh (2005)

reported that there are jarosite, goethite, hematite and limonite in oxidation zone of Darrehzar mine as well as Atapour and Aftabi (2007) mentioned that there is a range of goethite > hematite > jarosite in gossan and leached zone of Darrehzar.

Fortheremore, ICP-MS results on by Keshavarzi (2006) revealed high amounts of iron (Fe) in collected sediments of Darrehzar river.

The spectral analysis of collected samples spectra (taken from Darrehzar mine in 2015) also present the following results:

- Goethite is the most abundant mineral present in the collected samples so that there is it in most of the collected samples with high values (50 to 100%).

- The samples taken from the mining pit show medium (20 to 50%) and high (50 to 100%) values of hematite, while collected samples

from the tailing dumps present a low value (5 to 20%) of that.

- Jarosite is presented in the samples taken from Darrehzar mine area with low value (5 to 20%) (Figure 2 and Table 1).

The X-ray diffraction from rock samples correspond to the location of discriminated areas showed existence of jarosite and goethite specially inside the Darrehzar mine. These minerals are observed mainly with clay minerals in XRD analysis from rock samples (Seifi et al., 2019a).

Table 1: Characteristics of rock samples measured by ASD FieldSpec®3 spectroradiometer (The final percentage for minerals in the table were calculated by average percentage of minerals in results of PIMA View and Specmin-PRO).

	Mining Pit								
	Da1	Da2	Da3	Da4	Da5	Da6	Da21	Da24	
Goethite	56.08	0	47.43	62.72	58.09	27.37	41.83	26.03	
Hematite	0.59	0	0	0	41.91	35.43	58.17	50.92	
Jarosite	0	0	0	12.79	0	6.37	0	0	
Clay	43.33	100	52.57	24.49	0	30.83	0	23.05	

	Western Dump							Southern Dump	
	Da7	Da8	Da9	Da10	Da12			SD	SD1
Goethite	80.31	84.66	77.37	39.51	0		Goethite	77.81	82.1
Hematite	6.55	9.46	0	12.01	70.74		Hematite	3.16	2.66
Jarosite	0	0	0	0	0		Jarosite	6.16	0.48
Clay	13.14	5.88	22.63	48.48	29.26		Clay	12.87	14.76

|	Eastern Dump									
	Da26	Da27	Da28	ED1	ED2	ED3	ED4	NED	NED1	NED2
Goethite	72.07	65.54	75.69	72.75	59.39	78.91	61.75	53.52	68.29	51.18
Hematite	16.94	0	3.38	4.17	0	21.09	0	7.66	7.96	4.31
Jarosite	10.99	0	9.52	0	0	0	0	23.77	14.22	29.04
Clay	0	34.46	11.41	23.08	40.61	0	38.25	15.05	9.53	15.47

4.3. Change Detection

Subtraction Algorithm was implemented on the results of the previous step, mineral identification, in order to detect the changes of secondary iron minerals such as goethite, hematite and jarosite, as

well as statistical threshold (-0.5, -0.2, 0, 0.2, 0.5) was used to achieve better results. The result of change detection is based on the brightness of pixels in the initial and final states of images as ascending and descending of secondary iron

minerals (jarosite, goethite, and hematite) in the mine site during an 11-year period in red and in blue, respectively. Implementation of change detection algorithm at the area revealed that mining activities and geochemical conditions cause change in the surface by transferring minerals such as hematite, goethite, and jarosite. Goethite presents both increase and decrease in different areas of the mining pit and western, eastern, and southern tailing dumps, so that it shows the displacement of the goethite in the mine (Figure 6A). Hematite mainly shows a decrease in the area of mine but increases sporadically in the mining pit and the paths leading to the waste dumps (Figure 6B). Jarosite increases mostly in mining pit and in small parts of western, eastern and southern waste dumps.

The Darrehzar river is the most important place where jarosite is increased because the waste water reacts with pyrite and minerals such as jarosite are deposited. It should be mentioned that the surface water lake where the mine's acidic waters enter, is situated in the Darrehzar mine (Figure 6C). According to the history of the mine, the inactive western dump has been created and expanded during 1993 to 2010. This dump which is the oldest actually coincides with the exploration operations in 1993 (Yazdanpanah, 2011). The inactive eastern dump has been generated during 2010 to 2015. Furthermore, the active southern waste dump created in 2010 (unpublished data from the Darrehzar mine).
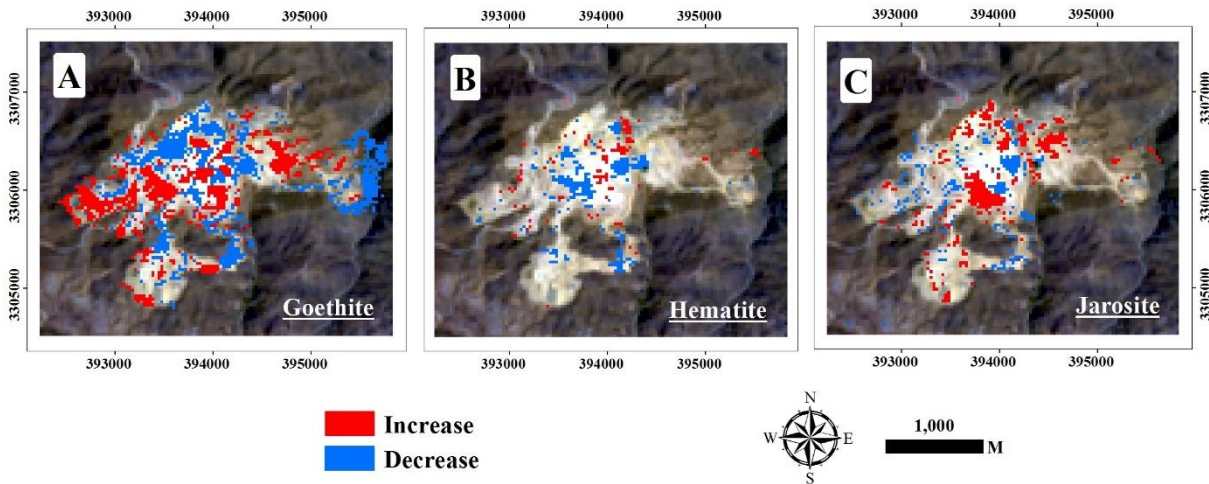
Figure 6. A) Result of the goethite change detection; B) Result of the hematite change detection; C) Result of the jarosite change detection. (Blue: decrease in jarosite, goethite and hematite; Red: increase in jarosite, goethite and hematite).

5. Conclusion

The employed method is practical to identify change of the secondary iron minerals includes three phases, method selection, mineral identification and change detection. Sub pixel methods determine approximate values of minerals in image's pixels. Among the results of the six methods, MF and CEM using USGS library, image and Field spectra, the result of the MF method and image spectra is the best method for secondary iron minerals identification. The results of secondary iron minerals identification

by MF method using images spectra have compatibility with the field data and laboratory analysis, so that the goethite is the most abundant secondary iron mineral in Darehazar mine area. Identifying target and detecting change of it allow users to find an effective technique for identifying the target material and apply it in the subtraction algorithm for change detection. The subtraction algorithm was performed on the results of the mineral identification stage for changes detection of secondary iron minerals and statistical threshold was used. Implementation of change detection algorithm at the area revealed that mining activities and geochemical conditions cause change in the surface by transferring minerals such as hematite, goethite, and jarosite. Applying this method can be suggestions for future research in material change detection.

6.References

Abdolzadeh M. Geochemical, Mineralization and Alteration Study of Darrehzar Copper Deposit (Kerman) [Dissertation]. Shiraz: Shiraz University.; 2005.

Abedi M, Norouzi GH, Fathianpour N. Mineral potential mapping in Central Iran using fuzzy ordered weighted averaging method. Geophysical Prospecting 2015; 63: 461–477.

Afify HA. Evaluation of change detection techniques for monitoring land-cover changes: A case study in new Burg El-Arab area. Alexandria Engineering Journal 2011; 50: 187–195.

Aleksandrowicz S, Turlej K, Lewiński S, Bochenek Z. Change Detection Algorithm for the Production of Land Cover Change Maps over the European Union Countries. Remote Sensing 2014; 6: 5976-5994.

Alimohammadi M, Alirezaei S, Kontak DJ. Application of ASTER data for exploration of porphyry copper deposits: A case study of Daraloo–Sarmeshk area, southern part of the Kerman copper belt, Iran. Ore Geology Reviews 2015; 70: 290–304.

Alizadeh Sevari B, Hezarkhani A. Hydrothermal evolution of Darrehzar porphyry copper deposit, Iran: evidence from fluid inclusions. Arab J. Geosci. 2014; 7: 1463–1477.

Atapour H, Aftabi A. The geochemistry of gossans associated with Sarcheshmeh porphyry copper deposit, Rafsanjan, Kerman, Iran: Implications for exploration and the environment. Journal of Geochemical Exploration 2007; 93: 47-65.

Basommi L, Guan Q, Cheng D. Exploring Land use and Land cover change in the mining areas of Wa East District, Ghana using Satellite Imagery. Open Geosci. 2015; 1: 618–626.

Beck R. EO-1 User Guide. Version 2.3. Ohio: University of Cincinnati; 2003.

Beiranvand Pour A, Hashim M, Genderen J. Detection of hydrothermal alteration zones in a tropical region using satellite remote sensing data: Bau goldfield, Sarawak, Malaysia. Ore Geology Reviews 2013; 54: 181–196.

Beiranvand Pour A, Hashim M. Hydrothermal alteration mapping from Landsat-8 data, SarCheshmeh copper mining district, south-eastern Islamic Republic of Iran. Journal of Taibah University for Science 2015; 9: 155–166.

Boardman JW, Kruse FA, Green RO. Mapping target signatures via partial unmixing of AVIRIS data. In: Proceedings of the Fifth JPL Airborne Earth Science Workshop; 1995; Pasadena, California.

Department of the Interior U.S. Geological Survey. Landsat 8 (L8) Data Users Handbook. Version 2.0. Dakota: Earth Resources Observation and Science (EROS) Center; 2016.

ENVI 5.3 online help. Available at: file: /Exelis/ENVI53/classic/help/ENVI3WHelp.htm.

Farrand WH, Harsanyi JC. Mapping distributed geological and botanical targets through constrained energy minimization. Proceedings, 10th Thematic Conference on Geological Remote Sensing, San Antonio, TX, 9–12 May 1994, I-419–I-429.

Farrand WH, Harsanyi JC. Mapping the distribution of mine tailings in the Coeur d'Alene River Valley, Idaho, through the use of a constrained energy minimization technique. Remote Sens. Environ. 1997; 59 (1): 64–76.

Gabr S, Ghulam A, Kusky T. Detecting areas of high-potential gold mineralization using ASTER data. Ore Geology Reviews 2010; 38: 59–69.

Geological Survey of Iran. Exploration for ore deposit in Kerman Region. Report Y/53. Tehran: Geological Survey of Iran; 1973.

Ghulam A, Amer R, M. Kusky T. Mineral Exploration and Alteration Zone Mapping in Eastern Desert of Egypt Using ASTER Data. In: ASPRS 2010 Annual Conference; 2010 April 26-30; San Diego, California.

Guo Y, Huang P, Zhang W, Yuan X, Fan F, Wang H, Liu J, Wang Z. Leaching of heavy metals from Dexing copper mine tailings pond. Trans. Nonferrous Met. Soc. China 2013; 23: 3068− 3075.

Harsanyi JC, Chang CI. Hyperspectral Image Classification and Dimensionality Reduction: An Orthogonal Subspace Projection Approach. IEEE transactions on geoscience and remote sensing 1994; 32(4): 779-785.

Harsanyi JC, Farrand WH, Chang CI. Detection of subpixel signatures in hyperspectral image sequences. Proceedings of 1994 ASPRS Annual Conference, Reno, Nevada 1994; 236–247.

Hosseinjani Zadeh, M. Evaluation of relationship between alteration and mineralization using spectral analysis and processing of multispectral and hyperspectral satellite data, case study middle part Dehaj-Sarduyeh, Kerman, South-East Iran [Dissertation]. Shiraz: Shiraz University; 2013.

Hosseinjani Zadeh M, Tangestani MH, Velasco Roldan F, Yusta I. Mineral Exploration and Alteration Zone Mapping Using Mixture Tuned Matched Filtering Approach on ASTER Data at the Central Part of Dehaj-Sarduiyeh Copper Belt, SE Iran. IEEE Journal of Selected Topics in Applied Earth Observations and Remote Sensing 2014a; 7(1): 284-289.

Hosseinjani Zadeh MH, Tangestani M, Roldan FV, Yusta I. Sub-pixel mineral mapping of a porphyry copper belt using EO-1 Hyperion data. Advances in Space Research 2014b; 53: 440–451.

Im J, Rhee J, Jensen JR, Hodgson ME. An automated binary change detection model using a calibration approach. Remote Sensing of Environment 2007; 106: 89–105.

ITT Visual Information Solutions. FLAASH Module User's Guide. Version 4.5.; 2008.

Keshavarzi B. Study of acid mine drainage in Darrehzar copper deposit and its environmental impacts [Dissertation]. Kerman: Shahid Bahonar University; 2006.

Kruse FA, Lefkoff AB, Boardman JW, Heidebrecht KB, Shapiro AT, Barloon PJ, Goetz AFH. The Spectral Image Processing System (SIPS) – Interactive Visualization and Analysis of Imaging Spectrometer Data. Remote Sensing of Environment 1993; 44: 145–163.

Lencioni DE, Hearn DR, Digenis CJ, Mendenhall JA, Bicknell WE. The EO-1 Advanced Land Imager: An Overview. Lincoln Laboratory Journal 2005; 15: 165-180.

Lobo FL, Costa MPF, Novo, EMLM. Time-series analysis of Landsat-MSS/TM/OLI images over Amazonian waters impacted by gold

mining activities. Remote Sensing of Environment 2014; xxx: 1-15.

Lu D, Mausel P, Brondi`zio E, Moran E. Change detection techniques. International Journal of Remote Sensing 2004; 25(12): 2365–2407.

Mendenhall JA, Lencioni DE, Hearn DR, Parker AC. EO-1 Advanced Land Imager in-flight calibration. Proc. SPIE 1998; 3439: 416-422.

Moazzen zadeh M, Tabatabaei SA, Hasani Mahmouei H. Investigation the causes of acid mine drainage copper production in Darrehzar mine and its control methods. In: 6nd Congress Health and Safety Executive in mining; 2006; Tehran, Iran.

Moen Vaziri H. history of Iran magmatism. 2nd ed. Tehran: Tarbiat Moallem University Press; 2004.

Mokhtari Z, Seifi A. Detection of Hydrothermal Alteration Zones Using ASTER Remote Sensing Data in Turquoise mine of Neyshabur. Journal of Analytical and Numerical Methods in Mining Engineering 2021; 11(28): 1-22.

Nateghi A, Hezarkhani A. (2013). Fluid inclusion evidence for hydrothermal fluid evolution in the Darreh-Zar porphyry copper deposit, Iran. Journal of Asian Earth Sciences 2013; 73: 240–251.

Navarro Torres VF, Aduvire O, Singh RN. Assessment of natural attenuation of acid mine drainage pollutants in El Bierzo and Odiel basins: A case study. Journal of Mining & Environment 2011; 2: 78-85.

Ololade O, Annegarn HJ, Limpitlaw D, Kneen MA. Land-use/cover Mapping and Change Detection in the Rustenburg Mining Region Using Landsat Images. In: IGARSS; 2008; Boston, MA, USA.

Parsapoor A. the study of petrography, petrology and hydrothermal alteration of Darrehzar copper porphyry deposits and relation between rock units with copper and molybdenum ore (Kerman, southeast Iran)

[Dissertation]. Isfahan: University of Isfahan; 2014.

Paterson N. Remote Mapping of Mine Wastes. In edited by A.G. Gubins. Proceedings of Exploration 97: Fourth Decennial International Conference on Mineral Exploration; 1997; 905–916.

Petropoulos GP, Partsinevelos P, Mitraka Z. Change detection of surface mining activity and reclamation based on a machine learning approach of multi-temporal Landsat TM imagery. Geocarto International 2012; iFirst article: 1-20.

Prakash A, Gupta RP. Land-use mapping and change detection in a coal mining area a case study in the Jharia coalfield. Int. J. Remote Sensing. 1998; 19(3): 391-410.

Ranjbar H, Hassanzadeh H, Torabi M, Ilaghi O. Integration and analysis of airborne geophysical data of the Darrehzar area, Kerman Province, Iran, using principal component analysis. Journal of Applied Geophysics 2001; 48: 33-41.

Ranjbar H, Honarmand M, Moezifar Z. Application of the Crosta technique for porphyry copper alteration mapping, using ETM$^+$ data in the southern part of the Iranian volcanic sedimentary belt. Journal of Asian Earth Sciences 2004; 24: 237–243.

Research System Inc. ENVI User's Guide. Version 4.1.; 2004.

Resmini RG, Kappus ME, Aldrich WS, Harsanyi JC, Anderson M. Mineral mapping with hyperspectral digital imagery collection experiment (HYDICE) sensor data at Cuprite, Nevada, USA. Int. J. Remote. Sens. 1997; 18 (7), 1553–1570.

Rowan LC, Hook SJ, Abrams MJ, Mars JC. Mapping Hydrothermally Altered Rocks at Cuprite, Nevada, Using the Advanced Spaceborne Thermal Emission and Reflection Radiometer (ASTER), A New Satellite-

Imaging System. Economic Geology 2003; 98: 1019–1027.

Sadeghi B, Khalajmasoumi M, Afzal P, Moarefvand P, Bijan Yasrebi A, Wetherelt A, Foster P, Ziazarifi A. Using ETM+ and ASTER sensors to identify iron occurrences in the Esfordi 1:100,000 mapping sheet of Central Iran. Journal of African Earth Sciences 2013; 85: 103–114.

Schroeter L, Gläβer C. Analyses and monitoring of lignite mining lakes in Eastern Germany with spectral signatures of Landsat TM satellite data. International Journal of Coal Geology 2011; 86: 27-39.

Seifi A, Esmaeily A, Mokhtari Z. A new hybrid method for epithermal gold exploration using multi-sensor satellite data in Sistan and Baluchestan Province (Iran). Ore Geology Reviews 2021; 138: 104357.

Seifi A, Hosseinjanizadeh M, Ranjbar H, Honarmand M. Detection of acid drainage using Landsat 8 image, Sarcheshmeh and Darrehzar mines, Kerman Province. In: Proceedings of the 34th National and the 2nd International Geosciences Congress; 2016; Tehran, Iran.

Seifi A, Hosseinjanizadeh M, Ranjbar H, Honarmand M. Investigation acid mine drainage minerals using spectral characteristics and satellite images processing of Landsat- 8, a case study: Darrehzar mine, Kerman province, Iran. Journal of Environmental Studies 2017; 43(1): 31–43.

Seifi A, Hosseinjanizadeh M, Ranjbar H, Honarmand M. Identification of Acid Mine Drainage Potential Using Sentinel 2a Imagery and Field Data. Mine Water and the Environment 2019a; 38: 707–717.

Seifi A, Hosseinjanizadeh M, Ranjbar H, Honarmand M. Visible-Infrared spectroscopy and chemical properties of water in mining area. Water Science & Technology 2019b; 80(9): 1612–1622.

Settle J, On constrained energy minimization and the partial unmixing of multispectral images. IEEE transactions on geoscience and remote sensing, 2002; 40(3), 718-721.

Shahriari H, Ranjbar H, Honarmand M. Image Segmentation for Hydrothermal Alteration Mapping Using PCA and Concentration–Area Fractal Model. Natural Resources Research 2013; 22(3): 191-206.

Singh B, Wilson MJ, Mchardy WJ, Fraser AR, Merrington G. Mineralogy and chemistry of ochre sediments from an acid mine drainage near a disused mine in Cornwall, UK. Clay Minerals 1999; 34: 301-317.

Townsend PA, Helmers DP, Kingdon, CC, McNeil BE, de Beurs KM, Eshleman KN. Changes in the extent of surface mining and reclamation in the Central Appalachians detected using a 1976–2006 Landsat time series. Remote Sensing of Environment 2009; 113: 62-72.

Vali A, Mokhtari F, Moayyeri M, Amini A. Anteropogeomorphology of mines landscape (Case Study: Crushed Lashtar). Quantative Geomorphology Researches 2014; 2: 104-116.

Valizadeh Kamran K, Khorrami B. (2018). Change Detection and Prediction of Urmia Lake and its Surrounding Environment During the Past 60 Years Applying Geobased Remote Sensing Analysis. The International Archives of the Photogrammetry, Remote Sensing and Spatial Information Sciences; 2018; Istanbul, Turkey.

Wen X, Yang X. A New Change Detection Method for Two Remote Sensing Images based on Spectral Matching. In: International Conference on Industrial Mechatronics and Automation; 2009 15-16 May; Chengdu, China. DOI: 10.1109/ICIMA.2009.5156567.

Yazdanpanah L. Analysis of geochemical data in Darrehzar copper deposit: using GIS software and remote sensing [Dissertation]. Kerman: Shahid Bahonar University; 2011.

Yucel DS, Yucel MA, Baba A. Change detection and visualization of acid mine lakes using time series satellite image data in geographic information systems (GIS): Can (Canakkale) County, NW Turkey. Environ Earth Sci. 2014; 72: 4311-4323.

Zabcic N. Derivation of surface pH-values based on mineral abundances over pyrite mining areas with airborne hyperspectral data (Hymap) of Sotiel-Migollas mine complex [Dissertation]. Spain: University of Alberta; 2008.

Zhang X, Pazner M, Duke N. Lithologic and mineral information extraction for gold exploration using ASTER data in the south Chocolate Mountains (California). ISPRS Journal of Photogrammetry & Remote Sensing 2007; 62(4): 271–282.